Piotr PUTEK[1], Piotr PAPLICKI[2], Marian SLODIČKA[1], Ryszard PAŁKA[2] and Roger VAN KEER[1]

Ghent University, *Nam*[2] Group, Department of Mathematical Analysis (1), West Pomeranian University of Technology, Szczecin, Department of Power Systems and Electrical Drives (2)

Application of topological gradient and continuum sensitivity analysis to the multi-objective design optimization of a permanent-magnet excited synchronous machine

Streszczenie. *W artykule przedstawiono zastosowanie metody gradientu topologicznego oraz zmiennej sprzężonej w zagadnieniu optymalizacji maszyn elektrycznych z magnesami trwałymi. Opis metody, jej funkcjonowanie oraz uzyskane wyniki symulacji numerycznych przedstawiono na przykładzie optymalizacji silnika z magnesami trwałymi o regulowanym wzbudzeniu, przewidzianego do napędu samochodów elektrycznych. Celem badań było wyznaczenie optymalnej geometrii biegunów silnika, utworzonych przez magnesy trwałe oraz elementy żelazne. Na podstawie przeprowadzonych obliczeń numerycznych w przestrzeni 2D wykazano efektywność prezentowanej metody, przy pomocy której wyznaczono optymalny kształt biegunów magnetycznych silnika. W celu weryfikacji otrzymanych wyników obliczeniowych, opracowano adekwatne modele trójwymiarowe maszyny, które poddano szczegółowej analizie. Na podstawie analizy porównawczej wyników badań na modelach 3D, wykazano możliwość znacznego zmniejszenia momentu zaczepowego, masy magnesów trwałych oraz poziomu wyższych harmonicznych w napięciu indukowanym w uzwojeniach twornika.*

Abstract*. The paper presents an application of the topological derivative and continuum sensitivity analysis for the optimal design of the permanent magnet excited machines. The description of the method, applications and numerical results are presented in an example of the optimization of the permanent magnet machine with the adjustable excitation which can be used as a drive for electrical vehicles. The purpose of this study was the determination of the optimum geometry of motor poles, formed by the permanent magnets and iron elements. On the basis of numerical calculations in the 2D space the efficiency of the method was demonstrated, determing the optimal shape of the magnetic poles of the motor. In order to verify results, three-dimensional models were developed and analyzed in details. Based on the comparative analysis of 3D results it has been shown that a significant reduction of the cogging torque, magnets weight and a level of higher harmonics in the voltage induced in the armature windings are possible. (**Zastosowanie gradientu topologicznego oraz metody zmiennej sprzężonej do wielokryterialnej optymalizacji kształtu maszyny synchronicznej z magnesami trwałymi**).*

Słowa kluczowe: optymalizacja struktury maszyny z magnesami trwałymi, minimalizacja momentu zaczepowego, gradient topologiczny, analiza wrażliwości.
Keywords: topology optimization of PM excited machine, minimization of cogging torque, topological gradient, sensitivity analysis.

Introduction

The permanent magnet (PM) synchronous machines due to their high torque per mass, high power per unit volume and high efficiency have found a broad use in industry, especially in automotive field for driving electric vehicles. The special properties of PM motors like low level of noise make them suitable for such type of applications. There are many studies and publications corresponding to PM synchronous machines e.g. [1-2]. Summarizing, it can be said that there are many designs of PM motors which guarantee to achieve the excellent efficiency of energy conversion, especially in the low speed range e.g. [3]. However, these constructions of motors can suffer in high speed regions due to the limited battery-voltage which is certainly a common drawback. There are various solutions of this problem, for example [4-5].

For this purpose the special construction called Electric Controlled Permanent Magnet Excited Synchronous Machine (ECPSM) invented by authors [6] was investigated. The machine topology is depicted in Fig.1. It consists of PM excitation, single teeth winding and an additional circumferential excitation coil (auxiliary coil) fixed on the stator in the axial center of the machine between pole structures of the rotor. By proper driven of the auxiliary coil using e.g. 2Q-DC chopper it is possible to control the effective excitation field, which produces induced voltages limited only by the saturation of the iron core in the armature winding between zero and maximum value. The main data of the machine are given in Table 1. This work focuses on the optimization of above-mentioned ECPSM structure. The mail goal is to minimize the CT assuming that the controlled magnetic flux density may reach quite different values.

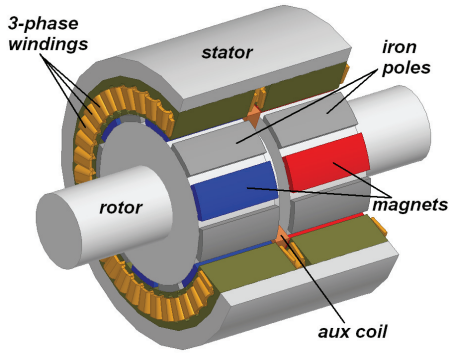

Fig.1. ECPSM with the surface-mounted PM rotor and stator structure exhibiting 3-phase single-tooth windings with auxiliary coil

Table 1. The main parameters of ECPSM topology

$2p$: number of poles	12
r_{ostat}: outer radius of the stator	67,5 mm
r_{istat}: inner radius of the stator	41,25 mm
l_{as}: axial length one part of the stator	35 mm
w_{oslot}: width of the slot opening	4 mm
ns: number of slots	36,0
m: number of phases	3
t_m: thickness of magnets (NdFeB, $B_r = 1{,}2T$)	3,0 mm

Model description

The 2D finite-element model of the structure under consideration has been shown in Fig.2. Hence, the field distribution in the analyzed model can be described in the form of weak formulation with suitable test function φ as follows

$$(1)\quad \begin{cases} \left(\nu_0 \nabla\times\mathbf{A}, \nabla\times\boldsymbol{\varphi}\right) = \mathbf{0} & \text{in } \Omega_0, \\ \left(\nu_{PM}\nabla\times\mathbf{A}, \nabla\times\boldsymbol{\varphi}\right) = \left(\nu_{PM}\mathbf{M}, \nabla\times\boldsymbol{\varphi}\right) & \text{in } \Omega_{PM}, \end{cases}$$

where $\mathbf{A}$ means the magnetic vector potential, ν_0 and ν_{PM} are the reluctivity of the PM and the air, $\mathbf{M}$ stands for the permanent magnetization, while Ω_0 and Ω_{PM} specify the areas of the air gap and iron, as well as the permanent magnet, respectively. Moreover, the nonlinear characteristic of the reluctivity was neglected. Thus, for the calculation of cogging torque (CT) and numerical model the standard Finite Element (FE) analysis was used.

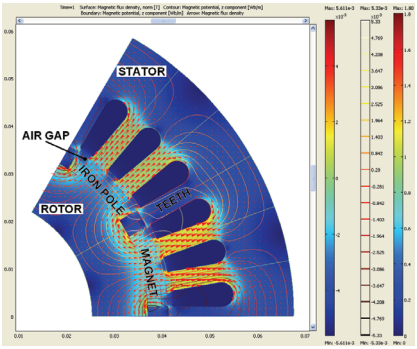

Fig.2. Magnetic flux norm (surface) and field lines (contours) calculated by Comsol 3.5

For computing of the torque, the Maxwell stress method was used [7]. In this approach the knowledge of the local flux density distribution along the contour is required. In this method the total electromagnetic force on the stator can be defined as

$$(2)\qquad \mathbf{F} = L_s \oint_l \left(\nu_0 \left(\mathbf{n}\cdot\mathbf{B}\right)\mathbf{B} - \frac{\nu_0}{2}\mathbf{B}^2\mathbf{n} \right) dl.$$

Here, L_s stands for the axial length of the stator, $\mathbf{n}$ means the normal direction, $\mathbf{B}$ is the flux density on the air surface, l means any closed path in the air gap surrounding the rotor. Finally under assumption of no-current armature and the fact that only the tangential component of the Maxwell stresses generates torque, the CT can be computed using

$$(3)\qquad T = r\cdot F_t = r\cdot L_s \oint_l \nu_0 B_n B_t dl,$$

where r is the radius of the circular path taken and t means the tangential component of Maxwell stress tensor.

Multi-objective cost function

Based on the expression (2) the following multi-objective function was defined for the optimization purpose

(4)

$$F(\mathbf{p}) = \mathbf{w}^T\mathbf{f} = \frac{1}{2}\left(w_1 \left\| T(\mathbf{p}) - T_0 \right\|_2^2 + w_2 \left\| \mathbf{B}(\mathbf{p}) - \mathbf{B}_0 \right\|_2^2 \right).$$

Here, $\mathbf{p}$ means the vector of optimized parameters in the analyzed model, while $\mathbf{w}$ is a vector of weight coefficients. In our case it was not necessary to use of the Pareto front method [8] in order to find the best compromise between both functions $\mathbf{f}$. It results from the fact, that both functions used as objective criterions are not reciprocally excluded themselves. It means that when the CT is minimized, it also implies the minimization of the magnetic energy in whole system and, in consequence, the decrease of the value of the flux magnetic density in air gap and iron as well. Thus, first the value of the flux magnetic was specified based on the technical requirements, and then during optimization process this value was monitored. When the value of the flux magnetic density in air gap and iron calculated in k-th iteration falls below assumed critical value the process of optimization was stopped. Hence, this value just plays a role of the second stopping criterion.

Topological derivative and shape optimization

For the purpose of solving the above-mentioned design magnetostatic problem in a numerically efficient way, the sensitivity-based topology algorithm was applied. The first definition of the topological gradient TG so-called *bubble method* originated from the work of Schumacher et al [9]

$$(5)\qquad G(\mathbf{r}) = \lim_{d\to 0} \frac{F_{obj}(\Omega \setminus B(\mathbf{r},d)) - F_{obj}(\Omega)}{\delta(\Omega)},$$

where $\delta(\Omega) = -\text{area}(B(\mathbf{r},d))$ and $\Omega\setminus B(\mathbf{r},d) = \{\mathbf{y}\in\Omega, \| \mathbf{y}-\mathbf{x} \|_2 \geq r\}$, $F_{obj}(\Omega)$ means a cost function defined in the domain Ω. However, the first topology-based algorithm was constructed by Cea [10], who extended the meaning of the classical shape gradient to the inside of the domain. In later works e.g. [11-13] the adaptation of adjoint variable method and the domain truncated method allowed to obtain the topological asymptotic expansion.

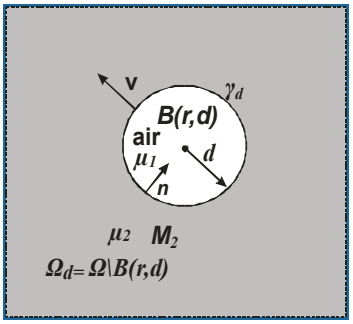

Fig.3. Design domain after cutting a small hole

In order to show the connection between the topological and classical shape sensitivity let us first consider the derivative of a scalar function $J(d, A_1)$ that is expressed by

$$(6)\qquad J(d, A_1) = F_{obj}\left(\Omega\setminus B(\mathbf{r},d), A_1\right),$$

where F_{obj} means the objective function defined in domain $\Omega\subset \mathrm{R}^2$, $B(\mathbf{r}, d)$ is a small hole centered in $\mathbf{r}\in\Omega$ with the radius d (Fig.3). Let A_1 be the solution of the partial differential equation describing the primary system (1). Additionally, it was assumed that a small perturbation, shown on Figure 3 in the large magnification, holds the outside boundary $\partial\Omega$ unchanged $\mathbf{V} = 0$ but causes an increase of radius d of the hole. It means that on the boundary γ_d velocity $\mathbf{V} = -\mathbf{n}$. Then, in a large class of formulations, also in case of magnetostatic design problems, the classical shape derivative of (5) in the direction $\mathbf{V}$ [14-15] can be calculated from

$$(7)\qquad J'(d, A_1, \lambda_2) = \int_{\gamma_d} \left(\mathbf{V}\cdot\mathbf{n}\right) L(A_1, \lambda_2) d\Gamma.$$

Here, $\mathbf{V}$ means the velocity, while $L(A_1, \lambda_2)$ is the scalar function defined on the boundary γ_d, which can be defined by an adjoint variable λ_2 and the potential A_1 describing the primary system. In order to calculate the function $L(A_1, \lambda_2)$ the continuum design sensitivity analysis can be used [16]. Thus, the classical shape sensitivity is expressed by (7), where function $L(A_1, \lambda_2)$ can be defined for two different materials as follows

(8) $$L_1(A_1,\lambda_2) = (\nu_1-\nu_2)\nabla\times A_1\cdot\nabla\times\lambda_2 \quad \text{in } \Omega_{d1}\setminus B_1(\mathbf{r},d),$$

(9) $$L_2(A_1,\lambda_2) = (\nu_1-\nu_2)\nabla\times A_1\cdot\nabla\times\lambda_2 + (M_2-M_1)\cdot\nabla\times\lambda_2 \quad \text{in } \Omega_{d2}\setminus B_2(\mathbf{r},d),$$

where functions L_1 and L_2 refer to the iron pole domain Ω_{d1} with the hole $B_1(\mathbf{r},d)$ or the PM pole region Ω_{d2} with $B_2(\mathbf{r},d)$, respectively. Finally, after some manipulation using the asymptotic analysis, the difference in the objective function before and after creating a hole takes the form of

$$J(\Omega\setminus B(\mathbf{r},d)-J(\Omega)=F_{obj}(\Omega\setminus B(\mathbf{r},d))-F_{obj}(\Omega)$$

(10) $$=-\int_0^d 4\pi\rho\cdot L(A_1,\lambda_2)d\rho=-2\pi d^2L(A_1,\lambda_2)+o(d^2).$$

Therefore, the topological gradient calculated in the center of a hole after combining (9) and (1) is given by

(11) $$G(\mathbf{r})=\begin{cases}2\cdot L_1(A_1,\lambda_2) & \text{in } \Omega_{d1}\setminus B(\mathbf{r},d)\\ 2\cdot L_2(A_1,\lambda_2) & \text{in } \Omega_{d2}\setminus B(\mathbf{r},d).\end{cases}$$

Concluding, the calculation of TG at any point of domain Ω requires only the FE analysis of the primary and dual system. Based on the optimality condition $G(\mathbf{r})=0$ on the hole boundary and $G(\mathbf{r})\le 0$ in Ω an algorithm for topological shape design is proposed [10].

Sensitivity-based topology algorithm

In the presented algorithm for the topological shape design also the area constraints was taking into account. The optimization procedure consists of the following steps:

1. The definition of problem that involves assumption of the objective function and the specification of an area constrain,
2. The determination of the design domain, which are comprised of the division of the initial domains into small cells, called voxels,
3. The FE analysis of primary and dual systems and setting the iteration counter k = 0,
4. The topology optimization involves:
   - the calculation of the TG in the center of all voxels,
   - sorting ascending voxels by the TG value,
   - removing material by the assumed area ratio (between 3% and 5% of the material area in each iteration)
5. The check of the convergence, if magnetic flux density has reached the critical value then stop procedure otherwise go to the next step,
6. The topology change that relies on checking the area constraint and then if unsatisfactory (k = k +1) and go to the step no 3.

Summarizing, the calculation of TG at any point of domain Ω mostly requires only the FE analysis of both considered models. It depends strongly on the minimized physical quantity. In case of the self-adjoint operators like e.g. energy both original and adjoint systems are the same. This fact was taking into account in our investigation on the design problem as well. On the other hand, such approach is also very efficient from computational viewpoint.

Numerical results

Considering the fact mentioned above the cost function was predefined (6) into the equivalent form as follows

(12) $$\overline{F}(\mathbf{p})=\mathbf{w}^T\overline{\mathbf{f}}=\frac{1}{2}\left(w_1\left\|W'(\mathbf{p})-W_0'\right\|_2^2+w_2\left\|\mathbf{B}(\mathbf{p})-\mathbf{B}_0\right\|_2^2\right).$$

where W' is the co-energy and W'$_0$ is a constant co-energy respectively. During searching the optimal parameters like the geometry of rotor poles, the mass factor, induced *emf* wave form and harmonics indicators, the sufficient and efficient approach was used. It relies on minimization of magnetic energy in a whole system in such direction that the flux density in the air gap can decrease according to assumed value, but an induced *emf* in the armature windings indicators will be still iteratively improved. Thus, the second stop criterion had to be introduced. When the flux density in the air gap or induced *emf* takes the 10% of rms value calculated for the initial configuration of PM machine, it has been assumed that the optimization process is completed.

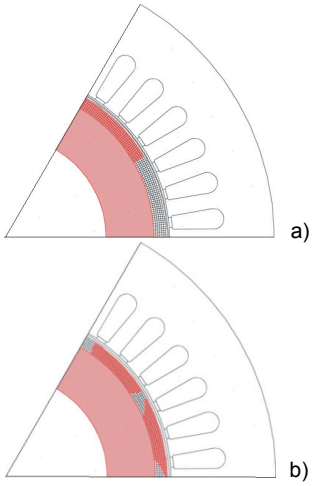

Fig.4. Course of the optimization process a) an initial structure of the one-pole pair, b) the shape of the one-pole pair in 7th iteration

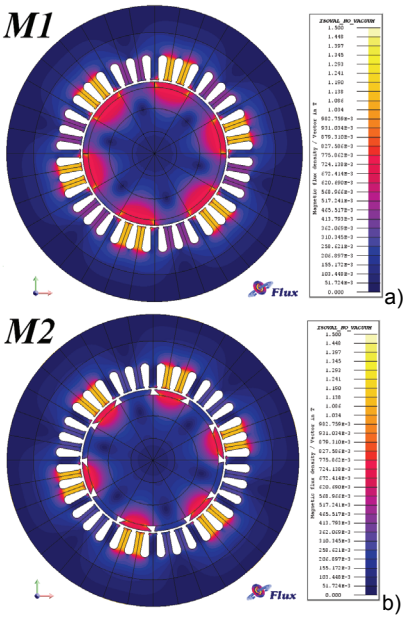

Fig.5. Magnetic field distribution within the M1 model and smoothed M2 (before and after optimization 2D)

In order to verify the result of optimization process in 2D model, first the full 3D model ECPSM structure was built and then the cogging torque for both structures – before and after optimization of rotor poles shape was

recalculated. In Fig.6 and 7 the cogging torque and induced *emf* in the armature windings for different currents of the auxiliary coil are shown.

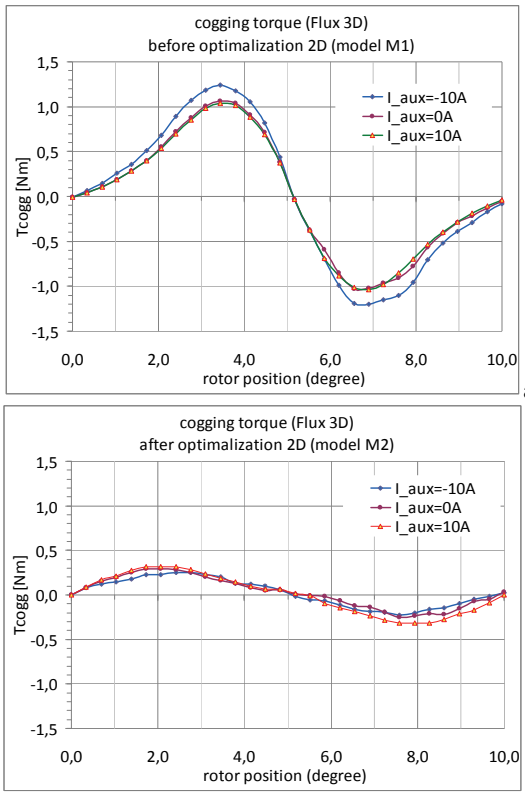

Fig.6. Cogging torque vs. rotor position for different DC-currents of the auxiliary coil i_{aux}

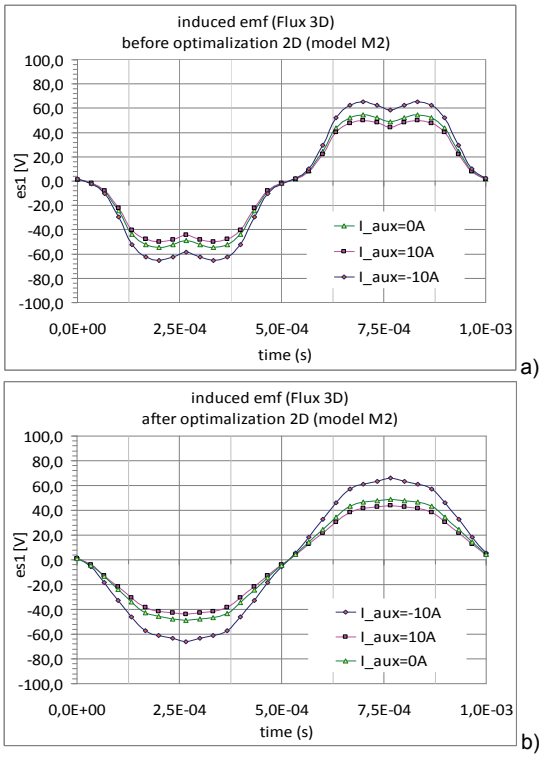

Fig.7. Induced *emf* in the armature windings vs. time for a rotor speed of 10000 rpm for different DC-currents of the auxiliary coil i_{aux}

Finally, some essential results of the optimization are summarized in Table 2, while the field distribution in both models, before and after optimization, are depicted in Fig.8.

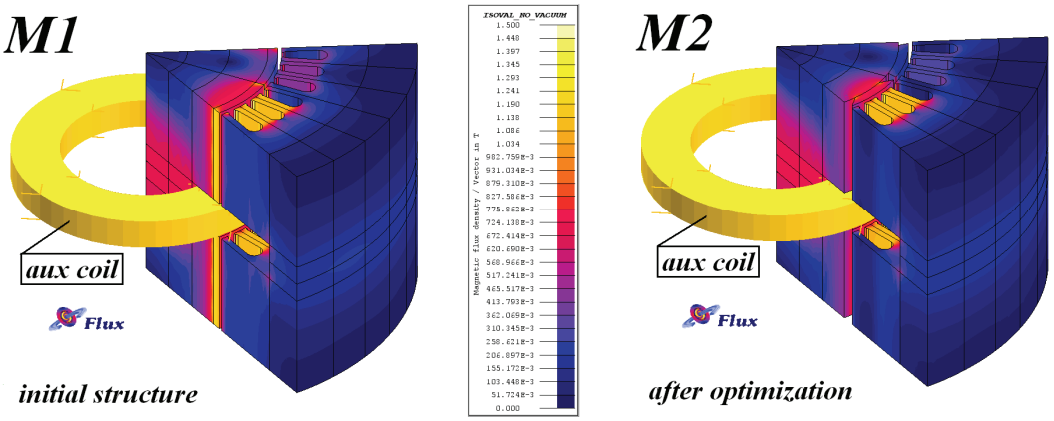

Fig.8. Magnetic field distribution in 3D model M1 (before optimization 2D) and M2 (after optimization 2D)

Table 2. Values of cogging torque, induced *emf*, magnetic flux density Br in air-gap in 3D models and mass of magnet/iron poles for different DC-currents of the auxiliary coil before model M1 and after optimization model M2

considerd quantities		M1-before optimization 2D			M2-after optimization 2D					
		I_{aux} [A] (DC-currents of the auxiliary)								
		- 10 [A]	0 [A]	10 [A]	- 10 [A]		0 [A]		10 [A]	
cogging torque [Nm]	T_cogg_mean	0,68	0,57	0,54	0,14	(79,6 %↓)	0,15	(74,3 %↓)	0,16	(69,9 %↓)
	T_cogg_RMS	0,79	0,67	0,65	0,16	(80,2 %↓)	0,17	(74,2 %↓)	0,20	(69,4 %↓)
	T_cogg_max	1,24	1,07	1,04	0,25	(79,7 %↓)	0,29	(72,7 %↓)	0,32	(69,3 %↓)
induced *emf* [V]	es1_mean	41,8	34,9	32,0	42,3	(1,1 %↑)	31,7	(9,0% ↓)	28,5	(11,2 %↓)
	es1_RMS	48,3	40,3	37,0	47,4	(1,8 %↓)	36,3	(9,9 %↓)	31,8	(14,0 %↓)
	es1_max	65,1	54,3	49,9	66,3	(1,8 %↑)	50,0	(7,9 %↓)	43,9	(12,0 %↓)
THD* *emf*		$15,5\ 10^{-2}$	$15,5\ 10^{-2}$	$15,7\ 10^{-2}$	$6,7\ 10^{-2}$	(57 %↓)	$6,7\ 10^{-2}$	(58 %↓)	$6,3\ 10^{-2}$	(60 %↓)
Br [T]	Br_rms	-	0,61	-	-	-	0,56	(8%↓)	-	-
mass [g]	magnet/iron poles	16,5/16,5			12,4	(25%↓)/14,4	(13%↓)			

**Total Harmonic Distortion of emf signal*

Figure 9 presents the magnetic flux density in the air gap.

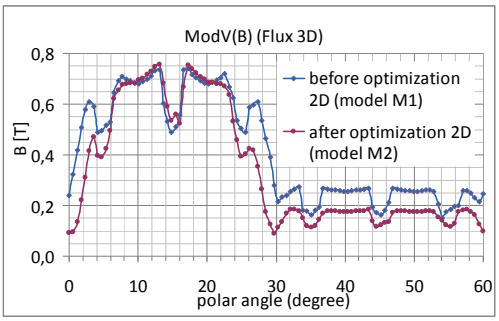

Fig.9. Magnetic flux density in the air-gap under magnet and iron pole without DC-currents of the auxiliary coil i_{aux}

Conclusions

The paper describes an application of the topological optimization with the continuum sensitivity analysis to the optimization of the magnetostatic design problem of a PM excited synchronous machine. This method allows to reduce the cogging torque in whole range of the auxiliary coil current, as well as to improve an induced *emf* wave form and harmonics of the initial structure of PM machine according to the assumed level of the magnetic flux density in the air gap and other quantities. This leads to reducing of the level of noise and vibration in the ECPSM structure. Additionally, the mass of the machine was also reduced. The main result for the optimization was summarized in Table 2. Based on the shown preliminary results for the simplified model, the full 3D design optimization of the new type machine approach for field weakening of permanent magnet has been provided. This proposed method has not been till now applied to simultaneously optimization of rotor poles made of two different materials.

Acknowledgements This work was partially supported by the projects IUAP P6/21 founded by Belgian Government, P. Putek is a postdoctoral researcher within the IUAP P6/21 ("Inverse problems and optimization in low frequency magnetism") and by the Ministry of Education and Science, Poland, under grant N N510 508040 (2011- 2013)".

REFERENCES

[1] Gieras J., Wing M., Permanent magnet motor technology, John Wiley & Sons, Ltd. (2008)
[2] Hughes A., Electric Motors and Drives, Elsevier Ltd. (2006)
[3] Husain I., Electric and hybrid vehicles. Design Fundamentals, CRC Press (2005)
[4] Tapia J., Leonardi F., Lipo T., Consequent-Pole Permanent-Magnet Machine with Extended Field-Weakening Capability, IEEE Transactions on Industry Applications, 39 (2003), 1704-1709
[5] Kabushiki Kaisha Meidensha, Hybrid Excitation Type Permanent Magnet Synchronous Motor, United States Patent, Patent Number: 5,682,073, Date of Patent: Oct. 28, 1997, Inventor: Takayuki Mizuno, Tokyo, Japan
[6] May H., Palka R., Paplicki P., Szkolny S., and Canders W.-R. Modified concept of permanent magnet excited synchronous machines with improved high-speed features, Archives of Electrical Engineering, 4 (2011), 531-540
[7] Chen N., HoS., and Fu W., Optimization of Permanent Magnet Surface Shapes of Electric Motors for Minimization of Cogging Torque using FEM, IEEE Transactions on Magnetics, 46 (2010), 2478-2481
[8] Di Barba P., Multiobjective Shape Design in Electricity and Magnetism, Springer (2010)
[9] Schumacher A., Kobolev V., Eschenauer H., Bubble method for topology and shape optimization of structures, J. Struct. Optimi. 8(1996) 42-51
[10] Cea J., Garreau S., Guillaume P., and Masmoudi M., The shape and topological optimizations connection, ELSEVIER Computer Methods in Applied Mechanics and Engineering, 118 (2000), 713-726
[11] Sokołowski J., Żochowski A., Topological derivatives for elliptic problems, Inverse Problems, 15 (1999), 123-124
[12] Garreau S., Guillaume P., Masmoudi M., The topological sensitivity for linear isotropic elasticity, European Conf. on Computational Mechanics (ECCM99), Raport MIP 99.45 (1999)
[13] Masmoudi M., Pommier P., and Samet B., The topological asymptotic expansion for the Maxwell equations and some applications, Inverse Problem 21(2005), 547- 564
[14] Sokołowski J., Zalesio J., Introduction to shape optimization: shape sensitivity analysis, Springer, (1992)
[15] Haug E., Choi K., Komkov V., Design Sensitivity Analysis of Structural Systems, Academic Press (1986)
[16] Kim D., Ship K., and Sykulski J., Applying Continuum Design Sensitivity Analysis combined with standard EM software to shape optimization in magnetostatic problems, IEEE Transactions and Magnetics, 40 (2004), 1156-1159
[17] Kim D., Sykulski J., and Lowther D., The implications of the use of composite materials in electromagnetic device topology and shape optimization, IEEE Transaction on Magnetics, 45 (2009), 1154-1156

***Authors**: dr inż. Piotr Putek, prof. dr hab. Marian Slodička, prof. dr. Roger Van Keer, pp@cage.ugent.be, ms@cage.ugent.be, rvk@cage.ugentbe, Department of Mathematical Analysis, Faculty of Engineering and Architecture, Ghent University, Galglaan 2, 9000 Gent, Belgium; dr inż. Piotr Paplicki, prof. dr hab. inż. Ryszard Pałka, paplicki@zut.edu.pl, rpalka@zut.edu.pl, Department of Power Systems and Electrical Drives, West Pomeranian University of Technology, Szczecin, ul. Sikorskiego 37, 70-313 Szczecin, Poland*